JOURNAL OF SYNCHROTRON RADIATION
ISSN 1600-5775

# Multipurpose end-station for coherent diffraction imaging and scattering at FERMI@Elettra free-electron laser facility

Flavio Capotondi,* Emanuele Pedersoli, Filippo Bencivenga, Michele Manfredda, Nicola Mahne, Lorenzo Raimondi, Cristian Svetina, Marco Zangrando, Alexander Demidovich, Ivaylo Nikolov, Miltcho Danailov, Claudio Masciovecchio and Maya Kiskinova

Elettra-Sincrotrone Trieste, SS 14 – km 163.5, Basovizza, Trieste 34149, Italy.
*Correspondence e-mail: flavio.capotondi@elettra.eu

Received 17 November 2014
Accepted 10 March 2015

Edited by I. Schlichting, Max Planck Institute for Medical Research, Germany

**Keywords:** coherent diffraction imaging; holography; scattering; free-electron laser; time-resolved experiments.

The Diffraction and Projection Imaging (DiProI) beamline at FERMI, the Elettra free-electron laser (FEL), hosts a multi-purpose station that has been opened to users since the end of 2012. This paper describes the core capabilities of the station, designed to make use of the unique features of the FERMI-FEL for performing a wide range of static and dynamic scattering experiments. The various schemes for time-resolved experiments, employing both soft X-ray FEL and seed laser IR radiation are presented by using selected recent results. The ongoing upgrade is adding a reflection geometry setup for scattering experiments, expanding the application fields by providing both high lateral and depth resolution.

## 1. Introduction

The advent of X-ray free-electron lasers (FELs) (Feldhaus, 2010; Emma *et al.*, 2010; Ishikawa *et al.*, 2012; Allaria *et al.*, 2012*a*, 2013*a*), generating very intense and coherent ultrashort pulses, has opened unique opportunities for lensless imaging techniques, based on coherent photon scattering. In the most widely used approaches, known as coherent diffraction imaging (CDI) and Fourier transform holography (FTH), the spatial and temporal correlations of the object are encoded into a speckle pattern of the far-field diffracted wave (Nugent, 2010). Using mathematical algorithms one can reconstruct the object from the pattern of the scattered light, which allows for exploring the properties of individual nano-objects or nano-sized building blocks of morphologically complex functional materials.

As demonstrated by the pioneering experiments at FLASH, the structural information of individual nano-objects is already captured in a single-shot FEL diffraction pattern, obtained within the femtosecond (fs) pulse duration that is shorter than the time when radiation damage is manifested (Chapman *et al.*, 2006). Later it was shown that single-shot CDI is also an excellent probe for exploiting transient states of the sample structure in 'classic' optical laser pump–FEL probe experiments (Barty *et al.*, 2008). Implementing a device for split and delay of the FEL pulses (Grübel *et al.*, 2007; Günther *et al.*, 2011), the dynamic properties of the objects under investigation can be studied by analyzing the temporal correlations between the scattered photons resulting from two consecutive FEL pulses. Apparently, all these time-resolved experiments explore the transient states with time resolution

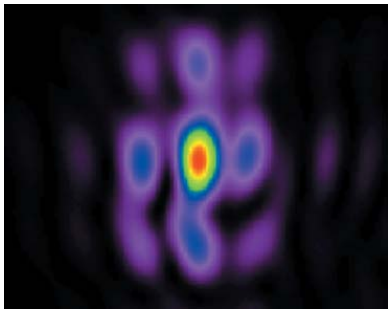

determined by the probe pulse duration, which at some of the FEL facilities can nowadays be pushed to a few tens of femtoseconds.

Stroboscopic nanometre imaging with femtosecond time resolution has opened unique opportunities to explore ultrafast dynamics, such as fracture, phase fluctuations, motions in soft matter, changes in various forms of magnetic or electronic segregations, copolymer assemblies, *etc*. Tuning the wavelength to a selected absorption edge for exploring resonant CDI (Song *et al.*, 2008; Tripathi *et al.*, 2011) adds local element specificity to the morphological information, thanks to the strong resonance enhancement of the scattering at the electronic transitions. In this respect the full transverse and longitudinal coherence and tunability of seeded FERMI-FEL pulses (Allaria *et al.*, 2012*a*,*b*) are the prerequisites for implementation of element-specific imaging modalities. The FERMI spectra purity and stability, combined with variable polarization (Allaria *et al.*, 2014), extend the information to spin and orbital momentum for revealing magnetic domain orientations, bond orientations, *etc*. For example, one of the most often used contrast mechanisms, based on X-ray circular dichroism (Van der Laan, 2013), has enabled exploitation of ultrafast dynamics of magnetic nano-domains (Müller *et al.*, 2013*a*,*b*).

The measurement station (Pedersoli *et al.*, 2011), operated at the FERMI beamline DiProI, was designed to host various setups in order to meet the requirements for all types of static and dynamic coherent scattering experiments, both in transmission and reflection geometry, namely (i) 'classical' CDI and FTH, for probing specimen structure with diffraction-limited resolution; (ii) resonant CDI and FTH for 'chemical' imaging, exploring 'dichroic' effects as well; (iii) time-resolved CDI and FTH for probing transient nanoscale dynamics from femtosecond to nanosecond timescales, using both optical laser and FEL pulses. The option for complementary projection imaging has also been considered, *i.e.* moving the sample out of focus provides shape information about the object and facilitates the iterative inversion of the diffraction pattern (Abbey *et al.*, 2008).

## 2. FEL and IR beamlines at FERMI

The DiProI end-station, hosted at a dedicated beamline that transports and tailors the FEL pulses to meet the stringent requirements of coherent scattering experiments, was commissioned in 2011–2012 (Capotondi *et al.*, 2013). Exploiting the advantage of a laser-seeded FEL, the IR pulses of the same Ti:sapphire laser used to trigger the FEL emission can also be delivered to the end-station through a dedicated IR 'beamline' and two optical breadboards. These IR pulses are intrinsically synchronized with the FEL and can be used as either a pump or a probe in almost jitter-free time-resolved experiments. Fig. 1 shows the general layout of the main components of the FEL and IR beamlines. Hereafter, we will briefly describe the core capabilities of the FEL and the IR beamlines: more detailed information is given elsewhere (Zangrando *et al.*, 2009; Raimondi *et al.*, 2013; Cinquegrana *et al.*, 2014; Danailov *et al.*, 2014).

### 2.1. FERMI-FEL photon transport

The photon analysis, delivery and reduction system consists of several units that secure the transport and the full control of the FEL beam, delivered to the currently operated end-stations at the LDM (Lyamayev *et al.*, 2013), DiProI and Timex (Masciovecchio *et al.*, 2015) beamlines. The beamlines share a common initial part and can be alternatively fed by the FEL-1 and FEL-2 light (spectral range 4–100 nm in the first harmonic), inserting a switching mirror. The FEL pulse intensity can be attenuated by more than three orders of magnitude using a gas cell, endowed with a couple of independent upstream and downstream $I_0$ monitors, recording the shot-to-shot intensity of the FEL radiation before and after attenuation (see Fig. 1). Additional attenuation of the FEL

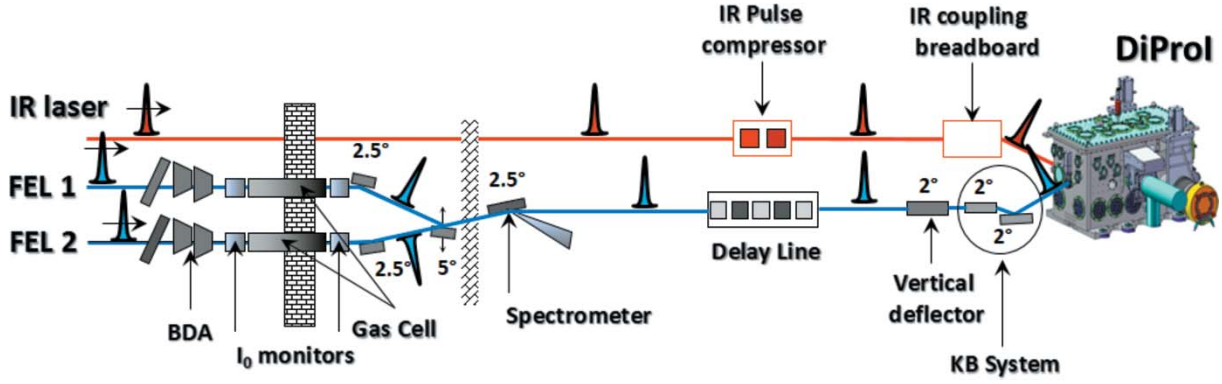


**Figure 1**
Layout of the FERMI-FEL and IR laser beamlines delivering FEL and IR light to the DiProI end-station. The FEL pulses, generated by two distinct FEL amplifiers (FEL-1 and FEL-2), are delivered to the DiProI end-station by the FERMI photon transport system. The FEL pulses can be tailored by the beam defining aperture (BDA) for removing the undulator off-axis emission. The FEL beam intensity can be monitored using two different ionization chambers ($I_0$ monitors). A gas cell, placed between the two $I_0$ monitors, can be used to reduce the intensity of the beam according to the experimental needs. The spectral content of the photons delivered to the end-station is monitored by a single-shot spectrometer along the photon transport systems. A split–delay line unit and an active Kirkpatrick–Baez (KB) system are additional optical elements for generating two FEL pulses with controllable delay for single color time-resolved experiments and to focus the beam onto the sample, respectively. Parallel to the EUV/soft X-ray beamline, there is an IR laser beamline that provides optical laser pulses for two-color experiments (IR pump–FEL probe or FEL pump–IR probe).

intensity and/or suppression of the seeding UV radiation is attained by inserting different solid-state filters (Al, Zr, Pd), placed along the common part of the beamlines.

After the first section, where the intensity of the FEL pulses is controlled, there is an online spectrometer providing single-shot information about the wavelength and the spectral quality of the FEL radiation (Allaria *et al.*, 2012*a*,*b*, 2013*a*). The spectrometer consists of two variable-line-spacing plane gratings with an overall resolving power better than $2 \times 10^4$, optimized for longer (100–24 nm) and shorter (28–3 nm) wavelengths, respectively (Svetina *et al.*, 2011). In addition to the on-line spectral information, the spectrometer can measure the absolute and the relative pulse intensity when the FEL is operating in two-color mode (Allaria *et al.*, 2013*b*; De Ninno *et al.*, 2013), used for FEL pump–FEL probe experiments (Allaria *et al.*, 2013*b*; Bencivenga *et al.*, 2014).

The common part of the beamlines after the spectrometer comprises a split-and-delay device, designed to split the FEL beam into two parts (using the edge of a grazing-incidence mirror) and subsequently recombine the two split beams on the same optical axis after their travel along adjustable length paths. The generated relative delay ranges from −2 ps up to 30 ps and is used for FEL pump–FEL probe experiments.

For increasing the pulse energy densities to several J cm$^{-2}$, required for investigation of very small objects in a single-shot mode, an active optical system based on two bendable mirrors in Kirkpatrick–Baez (KB) configuration is positioned before the DiProI station. The KB system has nominal focal lengths of 1750 mm (vertical) and 1200 mm (horizontal) and is designed to focus the FEL beam to a spot size of full width at half-maximum (FWHM) 5 µm × 6 µm for FEL-1 and of 4 µm × 5 µm for FEL-2 under the ideal condition of a pure Gaussian illumination (Raimondi *et al.*, 2013). However, owing to the relatively large beam divergence of FEL-1 and the presence of higher transversal modes in the emission of the source, the typical spot size during the experiment with FEL-1 is about 10 µm × 10 µm [see Fig. 2(*a*)]. This spot size can be diminished to ∼6 µm × 8 µm at the expense of the flux at the sample, by reducing the acceptance of the beam in front of the KB optics with manual baffles, as shown by the wavefront reconstruction in Fig. 2(*c*). The active nature of the optical focusing system also allows varying the spot shape and size for uniform illumination of larger areas.

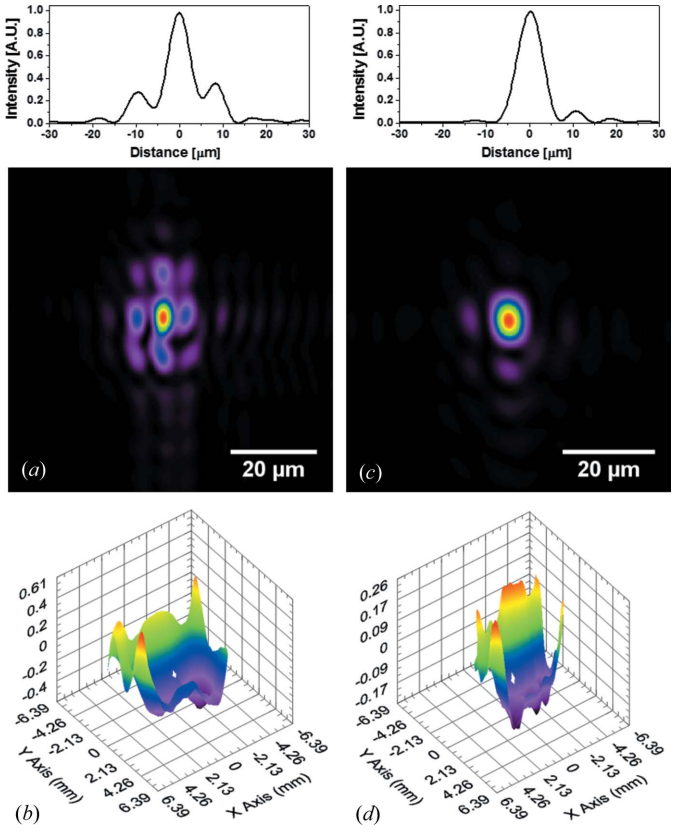


**Figure 2**
(*a*) Reconstructed FEL spot size for λ = 32 nm, using a wavefront sensor detector placed 950 mm downstream of the KB optics focal plane. (*b*) Distortion of the FEL wavefront owing to the high-order transversal mode, emitted by the source, and optic imperfections were measured to be 0.25λ RMS and 1.2λ peak-to-valley (PV). (*c*) Reconstructed spot size in the same experimental condition as (*a*) obtained defining the beam before the KB optics with mechanical baffles; the suppression of the high-order modes emitted by the source improves the spot quality into the focal plane and the flatness of the FEL wavefront to a distortion level of 0.13λ in RMS and 0.5λ in PV.

### 2.2. Optical laser transport

One of the prerequisites for FERMI experimental stations is to meet all requirements for pump–probe experiments with femtosecond temporal resolution using both FEL and optical laser radiation. The current optical laser source for time-resolved experiments is the seed laser, used for FEL pulse generation as well. One part of the seed laser is transported to the end-stations through a 150 m-long optical beamline, where the implementation of Rayleigh imaging and beam position-active stabilization enables the delivery of pulses with a very high pointing stability and an added timing jitter as low as 3 fs root-mean square (RMS) (Cinquegrana *et al.*, 2014). Thus, the temporal jitter between the FEL and IR pulses is extremely small and is measured to be about 10 fs inside the DiProI chamber (Danailov *et al.*, 2014). A compact pulse compressor, integrated in the beam transport, controls the pulse length in the range 90–250 fs.

As illustrated in Fig. 3(*a*), three optical breadboards are available for laser beam manipulation, IR beam transport into the chamber and diagnostics. The first one, of size 900 mm × 600 mm, provides different options for matching the optical pulse parameters to the experiment. An optical attenuator (Atten), made of a half-wave plate and two thin-film polarizers, is used to adjust the exact pulse energy impinging on the sample in the 1–700 µJ range (measured at En.). A translation stage (Sc.D) provides a variable pulse delay in the range ±570 ps. A compact single-shot auto-correlator (SSAC), built from a Fresnel prism, a thin BBO second-harmonic generation crystal and a CCD camera, is installed for input pulse duration diagnostics. The size of the beam at the sample can be adjusted by a lens telescope (T). The light polarization plane and state can be modified according to the experimental needs (WP). A green pilot laser (PL), installed on the breadboard, can assist

the preparation of the experiment when the seed laser is used by the other beamlines. After all parameters (energy, beam size, divergence and polarization) are set, the IR laser pulse passes on a 450 mm × 600 mm insertion breadboard with focusing lens and beam pointing stabilization system, compensating the beam pointing drifts. A compact second- and third-harmonic generation setup is available as well. Characterization of the transmitted or reflected beams after interacting with the sample can be made using the third 300 mm × 600 mm breadboard, placed at the output port of the chamber.

## 3. DiProI end-station

The DiProI end-station, sketched in Fig. 3(*a*), has a modular versatility that allows for different scattering experimental schemes for static and time-resolved experiments, both with fixed and free-standing objects. The station can host different experimental setups for performing experiments in transmission and/or reflection geometry using both FEL-1 and FEL-2 radiation and all possible pump–probe combinations using FEL and IR radiation. It has also an expansion module that can be added to use two detectors positioned at different distances behind the sample to simultaneously monitor small and large scattering angles.

### 3.1. Fixed sample experimental arrangements

The experimental setup for fixed solid samples, the only one used in 2012–2014, can be mounted on a 270 mm × 500 mm breadboard, placed on a high-load alignment stage that can move all mechanical components by ±2.5 mm in the *xyz* directions to precisely align the system with respect to the FEL beam axis. In order to reduce the stray radiation from the beamline, a set of motorized apertures with diameters ranging from 5 mm to 1 mm is placed on the input flange of the instrument. The entrance apertures, in combination with a similar set of motorized apertures on the rear part of the chamber, are commonly used to define the axis of the FEL beam using a HeNe laser. The latter can be positioned between the end-station and the KB optics chamber during the 'in air' installation and alignment of a desired experimental setup inside the vessel.

Fig. 3(*b*) shows the setup for forward-scattering CDI experiments. The sample, usually consisting of objects deposited on multiple $Si_3N_4$ membranes on a Si chip, is mounted on a four-axis stage that is able to align each target with respect to the FEL beam with a precision of 100 nm. The sample alignment can be visualized by means of a long-range optical telescope (5 µm resolution) mounted on top of the chamber using an in-vacuum viewer mirror at 45°, placed 35 mm upstream of the sample stage. The mirror also acts as additional protection for the detector from the beamline stray radiation, as the FEL beam passes through a 500 µm × 500 µm square aperture. Downstream of the sample holder, the incident FEL pulse is blocked by a 1 mm-diameter ball-shaped beamstop, placed at 35 mm from the sample holder. The scattered photons, after the interaction of the FEL pulses with the sample, are recorded on a 2048 × 2048 pixels Princeton Instrument MTE2048 CCD detector, mounted on a *xz* translation stage. This stage ensures complete removal of the detector from the FEL optical axis for using the diagnostics mounted on the rear part of the chamber, including bolometer and photodiodes, to measure the photon flux, and wavefront sensor, to monitor or optimize the beam spot size at the sample plane. The stage is also used for moving the detector along the optical axis of the FEL beam to vary the speckles angular separation. In the forward-scattering setup, the sample-to-detector distance can be varied from 55 mm (*i.e.* a maximum collection angle of ±14.5°) to 150 mm (maximum collection angle of ±5.1°). Owing to the presence of a fixed beamstop, the region of missing data at low exchanged momentum covers a range of about ±0.8° at the center of the diffraction pattern.

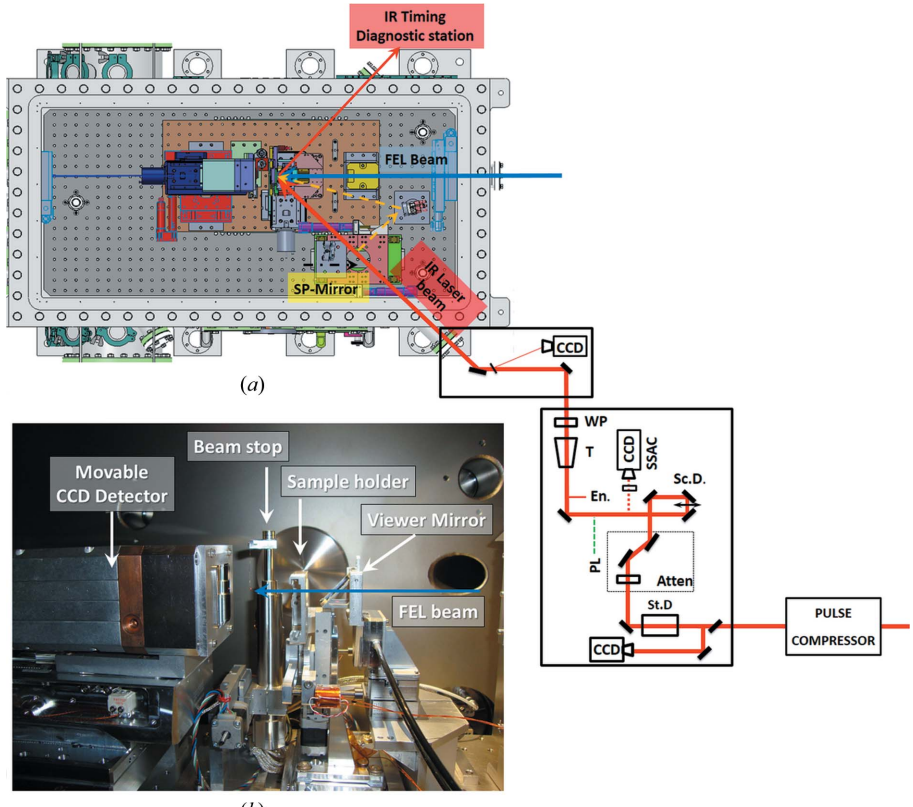


**Figure 3**
(*a*) Schematic layout of the DiProI end-station, including a detailed scheme of the delivery system for the IR seed laser beam after the pulse compressor. (*b*) Photograph of the forward-scattering setup with a single detector.

In time-resolved experiments using an optical IR laser, the detector can be light shielded by an ultrathin large-area film, directly mounted in front of the sensor chip. For this class of experiments, two optical laser paths have been conceived inside the vacuum vessel: the first one [red line in Fig. 3(*a*)], impinging on the sample plane at an angle of 45°, and the second one [orange dashed line in Fig. 3(*a*)], at an angle of 15°. The IR laser path inside the chamber can be switched without breaking the vacuum by inserting a movable second path (SP) mirror. Both the reflected beam for 45° geometry (red line in Fig. 3) and the transmitted beam through a $Si_3N_4$ thin film or membrane for the 15° one (not shown) can be used to determine the time coincidence between the FEL and the IR pulses with the timing diagnostic station placed outside the vacuum vessel. The 45° geometry is more suitable when one wants to push the temporal resolution in single-shot experiments by directly imaging the different arrival time of the tilted laser wavefront along the sample surface, so the sample dynamics can be mapped (Riedel *et al.*, 2013; Danailov *et al.*, 2014). However, the more collinear geometry is less affected by geometrical effects and has intrinsically better temporal resolution in laser pump–FEL probe experiments involving scanning of the laser delay line. Fig. 4 shows the changes of the optical reflectivity (red line) and transmission (blue) of a $Si_3N_4$ film, induced by FEL radiation, measured for the 45° and 15° geometry, respectively. Such measurements are routinely used to establish the temporal overlap between the two radiations. It is obvious that the smaller 15° angle geometry (initial fast drop about 200 fs) provides better temporal resolution compared with the larger 45° one (350 fs). As the IR laser beam derives from the same laser pulse used to seed the electron bunch (Cinquegrana *et al.*, 2014), typical measured arrival time jitter between the laser and the FEL at the sample plane is about 10 fs (Danailov *et al.*, 2014).

Another pump–probe setup that can be hosted inside the DiProI station is the recently developed compact FEL mini split–delay device (Bencivenga *et al.*, 2015) that allows the use of two FEL pulses in various configurations (Fig. 5*a*). The FEL beam can be split into two parts by the edge of a carbon-coated mirror ($M_0$), placed at a grazing incidence (3°) with respect to the incoming FEL beam. The two generated half FEL beams are recombined on the sample plane with an angle of 6°, by two successive 70 mm-long carbon-coated

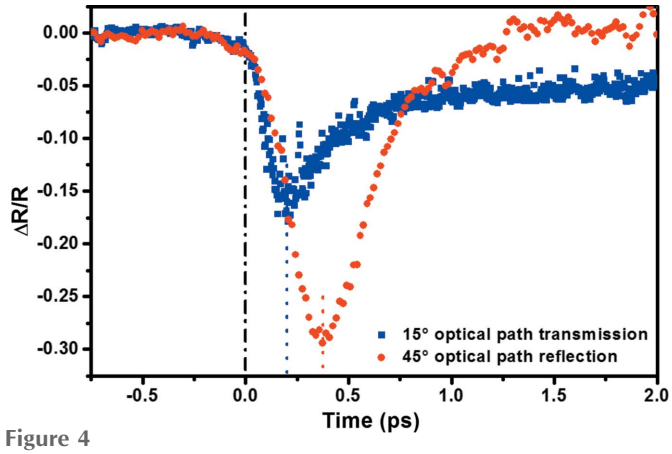


**Figure 4**
FEL-induced changes of optical reflectivity (red circles) and transmissivity (blue squares) of a $Si_3N_4$ sample. As indicated in Fig. 3(*a*), the IR laser pulses used for measuring the reflectivity and transmissivity have two different optical paths inside the DiProI chamber.

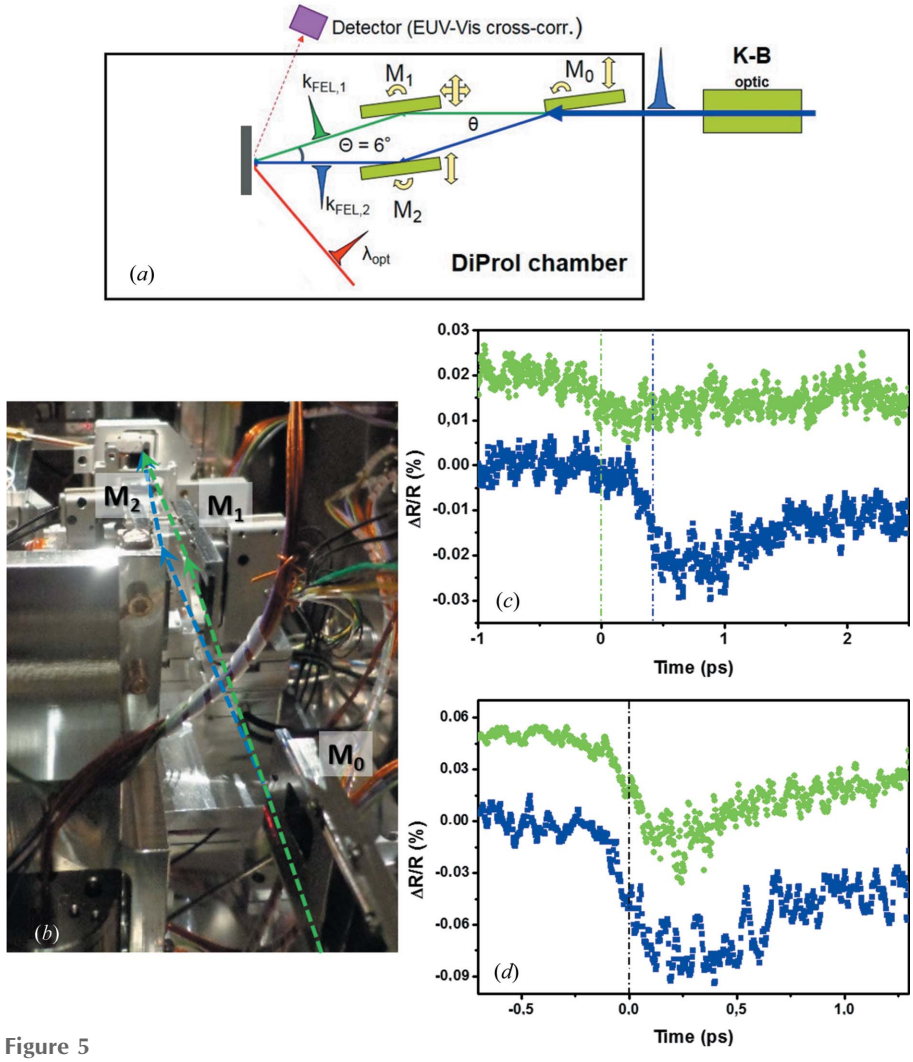


**Figure 5**
(*a*) Sketch of the mini split–delay setup incorporated inside the DiProI end-station. (*b*) Photograph of the setup: the edge of the mirror $M_0$ is used as a beam splitter and the two half-beams are recombined at the sample plane with an angle of about 6° by the mirrors $M_1$ and $M_2$. (*c*) FEL-induced reflectivity drop of $SiO_2$, measured by pumping either with the upper-branch FEL pulse (green) or with the lower-branch FEL pulse (blue), the upper pulse arriving about 450 fs before the lower one. (*d*) Same as (*c*), with upper and lower pulses arriving simultaneously.

mirrors ($M_1$ and $M_2$), placed in a parallelogram geometry. The beam direction can be controlled by means of piezo-electric stirring motors with a precision of about 50 µrad. Each of the two recombining mirrors ($M_1$ and $M_2$) can be aligned using linear piezomotors with a nominal resolution of 100 nm in the range ±9.5 mm [Fig. 5(*b*)]. The motors can be used to equalize the optical path of the two FEL beams, using a roto-translation of the mirror and keeping fixed the angle between the two beams on the sample plane. This enables a nominal scanning range of ±350 fs with respect to the nominal working position. The temporal coincidence or delay between the two half FEL beams can be controlled synchronizing each branch with the IR laser beam, probing the reflectivity drop induced by the FEL on dielectric material such as $Si_3N_4$ or $SiO_2$ in a reflection geometry cross-correlator. The plots of FEL-induced reflectivity changes in Figs. 5(*c*) and 5(*d*) illustrate the cases with the half-beam of the upper arm (green circles) arriving 450 fs before or simultaneously with the lower arm FEL (blue squares), respectively. The relative position of the mirror $M_0$ with respect to the incoming center of the FEL optical axis can be used to equalize the intensity of the two FEL beams by adjusting the optical reflectivity drop.

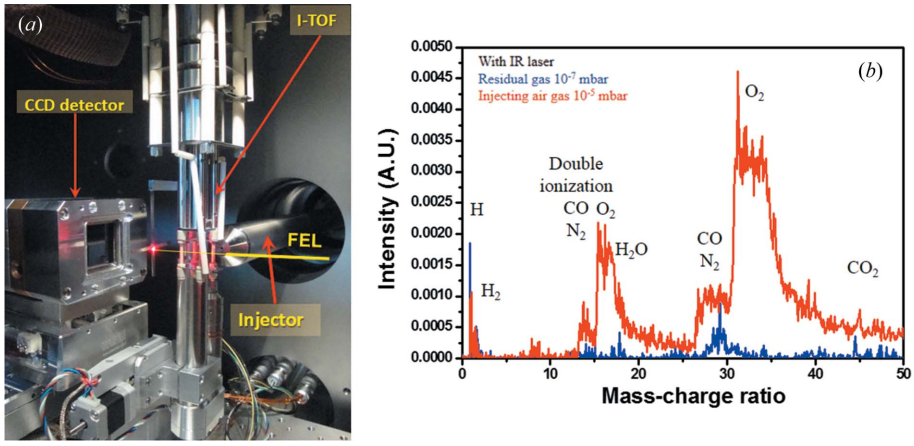


**Figure 6**
(*a*) Photograph of the experimental setup for CDI with airborne nanoparticles. (*b*) Time-of-flight spectra for a single-shot ionization of the residual gas inside the vacuum vessel by IR laser (blue curve) and when the injector is operating increasing the pressure to $10^{-5}$ mbar (red curve).

Owing to the slightly different impinging angle at the sample surface, this device is ideal to geometrically decouple the scattered photons on a far-field detector plane. This makes it possible to follow the time evolution of the diffraction speckle after a pumping FEL pulse (Günther *et al.*, 2011) or to collect two simultaneous diffraction patterns hitting the sample with two pulses at different angles. In the latter case, the two detectors encode simultaneously two different views of the sample, which is a promising approach to *three-dimensional imaging* without rotating the sample (Gleber *et al.*, 2009; Raines *et al.*, 2010; Xu *et al.*, 2014).

In brief, DiProI can exploit the mini-delay setup, the split-and-delay autocorrelator device and the two-color FEL schemes for studies of ultrafast dynamics in any combination of IR- or FEL-based pump–probe experiments.

### 3.2. Ancillary facilities for experiments with free-standing samples

For performing experiments with 'free-standing' nanoparticulate samples, the DiProI end-station can host a system composed of an aerosol particle injector, developed by J. Hajdu's group (Uppsala University) (Seibert *et al.*, 2011), combined with a time-of-flight (ToF) mass spectrometer. The vessel has a dedicated port for the particle delivery device [see Fig. 6(*a*)] that will be implemented and tested with the FEL-2 beam in the second semester of 2015. The system is designed to deliver objects with sizes ranging from 10 nm to 1000 nm, concentrated in a liquid carrier, guided in a 150 µm glass capillary. The latter is coupled at one end with a 350 µm glass capillary, carrying a high-pressure noble gas, to obtain an aerosol sample jet at atmospheric pressure. This jet is let into an expansion chamber with a variable differential pumping system, reducing the pressure down to 1 mbar, and then collimated into the experimental chamber through a series of aerodynamic lenses: six expansion chambers separated by round apertures, of diameter decreasing from 5 mm to 1.5 mm, aligned in a straight line. Most of the liquid carrier evaporates during this process, delivering into the interaction region in the FEL focus (10 mm from the injector end) a beam of free-standing nanoparticles collimated with a waist below 100 µm.

The flying objects are hit in the interaction region by the FEL and/or the IR pump laser and the diffraction patterns are monitored by the CCD. Simultaneously, the ToF mass spectrometer provides information about the products of sample ionization. In the ToF, the positively charged ions are accelerated in a high-voltage interaction cage (10 mm × 10 mm 4500 V repeller plate, 10 mm from the 10 mm × 10 mm 3500 V attractor grid, followed by ±200 V *xy* deflector plates), through a grounded 700 mm free-flight tube, to a micro-channel plate detector. The time-of-flight of the ions can be measured by an oscilloscope and the signal converted into mass spectra [see Fig. 6(*b*)] with a resolution expected to be better than 0.25 mass per charge units for particles lighter than 50 proton masses. The interaction cage has been miniaturized, to fit into the FEL interaction region between the CCD detector and the injector system, and customized with a large repeller–attractor distance to allow a wide CDI acquisition angle; this distance can be modified and optimized for different experimental setups for better uniformity of the accelerating field.

## 4. Overview of ongoing research projects

Following the first experiments during the commissioning period that demonstrated the possibility for single-shot CDI

(Capotondi *et al.*, 2013), a number of successful experiments were performed after opening the DiProI end-station to users at the end of 2012. Using a stack of purposely fabricated structures of galloping horses, Professor Chapman's group from CFEL has demonstrated the conformation sequence recovery from randomized single-shot diffraction patterns (Yoon *et al.*, 2014). A novel FTH approach with almost unrestricted reference choice was tested. The approach allows for optimizing the signal and resolution, and responding to the demands of resolution and fidelity required for single-shot imaging (Martin *et al.*, 2014).

One of the fields that has made significant advancements with the advent of the variable polarization FELs is magnetism and, in particular, identifying the mechanisms of ultrafast nanoscale magnetization switching, induced by femtosecond optical laser pulses. In this respect, taking FTH snapshots is a highly desirable approach for following the evolution of the structure of the magnetic domains after excitation. As exploring magnetic dynamics with FTH requires circularly polarized light, FERMI-FEL has attracted this user community. The first results that evidence ultrafast changes of the spatial magnetization profile, obtained in collaboration with scientists from TU-Berlin, DESY and CNRS, have already been published (Capotondi *et al.*, 2013; Müller *et al.*, 2013*b*; von Korff Schmising *et al.*, 2014).

The most recent IR pump/FEL probe study (von Korff Schmising *et al.*, 2014) explored the ultrafast demagnetization dynamics of a Co/Pd multilayer, induced by a deliberately spatially localized excitation *via* an optical standing wave. The measured temporal evolution of the profiles across the boundary between positive and negative magnetization domains has clearly shown an ultrafast increase of the profile width, by about 30 nm, 0.3 ps after the optical-induced demagnetization, compatible with superdiffusive spin transport. Another hot topic is exploring nonlinearity in resonant magnetic scattering cross section for high FEL pulse fluences, as it has to set the limits for the pulse lengths and delays used in the single-shot experiments. Provided the photoionization-induced energy shift (Müller *et al.*, 2013*a*) of the resonant transition is the reason for the reduced scattering efficiency, the ongoing FEL pump/FEL probe experiments with variable FEL pulse lengths and delays in the sub-50 fs range are expected to provide insights into the fundamental limits of these experiments.

The in-house research and development programs have exclusively been focused on the development of novel experimental schemes that open new opportunities for ultrafast science. We demonstrated in proof-of-principle diffraction experiments with a Ti grating the potential of two-color seeded FEL emission with independent control on relative intensity, time delay $\Delta t$ and photon wavelength difference $\Delta\lambda$ (Allaria *et al.*, 2013*b*). Using FEL pulses, tuned across the Ti *M*-edge, and varying the fluences of the FEL pump pulse, we showed the occurrence of FEL-induced transparency above a certain fluence threshold. The results are qualitatively described by changes of the optical constants at the wavelength of the probe and the fluence dependence and both the changes of absorption $\beta$ and refraction $\delta$ coefficients were evaluated (Allaria *et al.*, 2013*b*; Bencivenga *et al.*, 2014).

Thanks to the continuous implementation of new experimental schemes for exploring transient states of matter interacting with FEL pulses of variable wavelengths, intensities and pulse durations, we have made the first steps toward nonlinear wave-mixing experiments. These experiments should have a dedicated experimental station at the EIS-TIMER beamline in 2016 (Cucini *et al.*, 2011; Masciovecchio *et al.*, 2015) and some simplified schemes can be executed at DiProI as well. Very recently, using the mini-delay line, we have demonstrated for the first time the generation of a transient grating in a glass sample by hitting simultaneously the sample at different angles with the two split FEL pulses and probing with an optical laser pulse the induced electron density modulation (Bencivenga *et al.*, 2015).

## 5. Concluding remarks and outlook

In less than two years, the experimental station dedicated to CDI and scattering, operated at the DiProI beamline of the seeded FEL FERMI, has produced interesting results along with the continuous developing and implementing of new experimental schemes for expanding the research opportunities and pushing the spatial and temporal resolutions. The precise control and manipulation of both FEL and optical laser beams has provided users with a tool to perform almost jitter-free scattering experiments.

One of the planned activities is to develop and implement holography and CDI of airborne micro/nano objects sprayed in the FEL beam using defined reference structures, spatially decoupled from the flying samples. Owing to the full coherence of the FERMI pulses, the reference sample can be placed at sufficient distance from the injector tip ($\sim$1 mm estimated considering the longitudinal coherence length of FERMI pulses). The expected output is more reliable classification of the diffraction patterns and the phase-retrieving process.

The next step of major instrumental development is to implement, in 2015, a reflection scattering option. It will enable coherent scattering experiments with thicker specimens and exploitation of phenomena occurring at surfaces and interfaces as well (Roy *et al.*, 2011; Gardner *et al.*, 2012). Fig. 7 shows the new reflectometer designed in collaboration with C. Gutt's group (University Siegen). In this setup, under construction, the sample will be mounted on a five-axis ($x$, $y$, $z$, $\theta_y$, $\theta_z$) piezoelectric stage. The detector arm is fixed on a high-load rotatory stage, where either calibrated photodiodes for $\theta$–$2\theta$ rocking curve or a large area CCD can be hosted.

## 6. Facility access

The DiProI end-station is open to academia, government agencies and research institutes worldwide for scientific investigations in the area of ultrafast dynamic imaging and scattering. Access is obtained *via* peer-reviewed proposals.

More information about the core capabilities of the end-station, the research achievements and ongoing upgrades

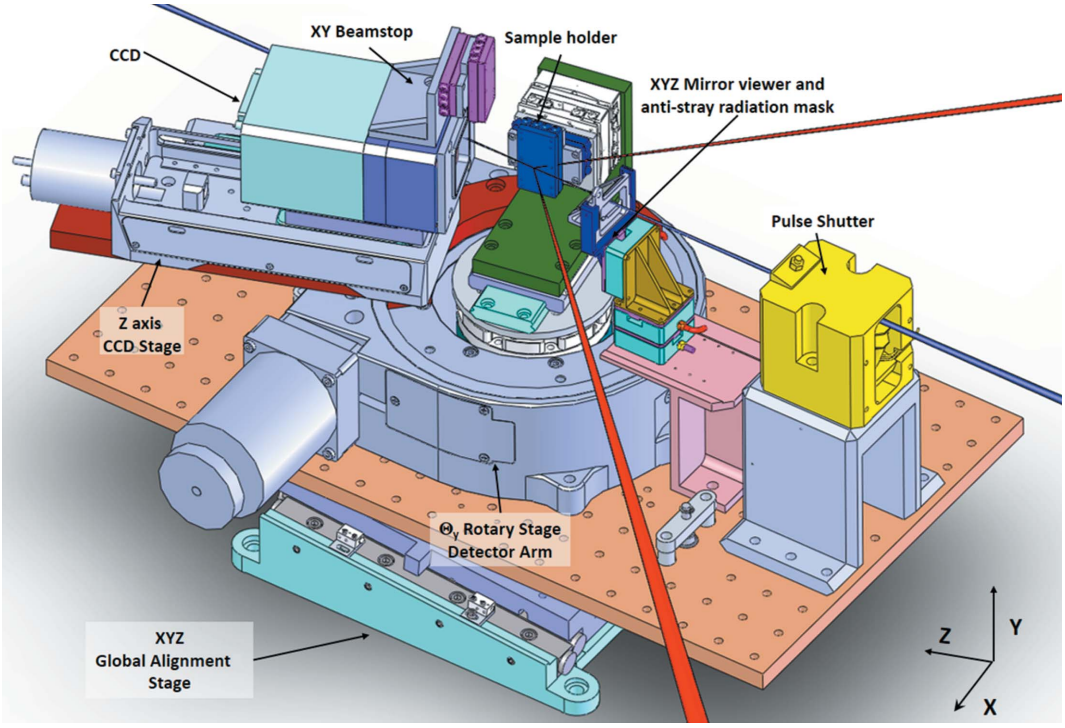


**Figure 7**
Design of the new DiProI setup and sample environment for reflection CDI.

can be found at http://www.elettra.trieste.it/lightsources/fermi/fermi-beamlines/diproi/diproihome.html.

## Acknowledgements

The design of the experimental station and the first commissioning experiments were carried out in close collaborations with LLNL, DESY and University of Uppsala. We are indebted to Henry Chapman (CFEL-DESY) and Janos Hajdu (University of Uppsala) and their groups for sharing their know-how and for their continuous help and support. Special thanks to Gerhard Grübel and his group in DESY who actively participated and advised the first commissioning magnetic imaging experiments. The fruitful discussions with Christian Gutt and his invaluable contributions in developing of the reflectivity setup are highly appreciated. The authors thank the FERMI Commissioning team for their valuable and dedicated support and are particularly grateful to L. Giannessi, E. Allaria, W. Fawley and M. Svandrlik. The work was partially funded by the FERMI project of Elettra-Sincrotrone Trieste, supported by MUIR grants FIRBRBAP045JF2 and FIRB-RBAP06AWK3, and by FVG regional grant NANOTOX 0060-2009.

## References

Abbey, B., Nugent, K. A., Williams, G. J., Clark, J. N., Peele, A. G., De Pfeifer, M. A., Jonge, M. & McNulty, I. (2008). *Nat. Photon.* **4**, 394–398.
Allaria, E. *et al.* (2012*a*). *Nat. Photon.* **6**, 699–704.
Allaria, E. *et al.* (2012*b*). *New J. Phys.* **14**, 113009.
Allaria, E. *et al.* (2013*a*). *Nat. Commun.* **4**, 2476.
Allaria, E. *et al.* (2013*b*). *Nat. Photon.* **7**, 913–918.
Allaria, E. *et al.* (2014). *Phys. Rev. X*, **4**, 041040.
Barty, A. *et al.* (2008). *Nat. Photon.* **2**, 415–419.
Bencivenga, F., Capotondi, F., Casolari, F., Dallari, F., Danailov, M. B., De Ninno, G., Fausti, D., Kiskinova, M., Manfredda, M., Masciovecchio, C. & Pedersoli, E. (2014). *Faraday Discuss.* **171**, 487–503.
Bencivenga, F. *et al.* (2015). *Nature (London)*. **520**, 205–208.
Capotondi, F. *et al.* (2013). *Rev. Sci. Instrum.* **84**, 051301.
Chapman, H. N. *et al.* (2006). *Nat. Phys.* **2**, 839–843.
Cinquegrana, P., Cleva, S., Demidovich, A., Gaio, G., Ivanov, R., Kurdi, G., Nikolov, I., Sigalotti, P. & Danailov, M. B. (2014). *Phys. Rev. ST Accel. Beams*, **17**, 040702.
Cucini, R., Bencivenga, F., Zangrando, M. & Masciovecchio, C. (2011). *Nucl. Instrum. Methods Phys. Res. A*, **635**, S69–S74.
Danailov, M. B. *et al.* (2014). *Opt. Express*, **22**, 12869–12879.
De Ninno, G., Mahieu, B., Allaria, E., Giannessi, L. & Spampinati, S. (2013). *Phys. Rev. Lett.* **110**, 064801.
Emma, P. *et al.* (2010). *Nat. Photon.* **4**, 641.
Feldhaus, J. (2010). *J. Phys. B*, **43**, 194002.
Gardner, D. F., Zhang, B., Seaberg, M. D., Martin, L. S., Adams, D. E., Salmassi, F., Gullikson, E., Kapteyn, H. & Murnane, M. (2012). *Opt. Express*, **20**, 7243–7254.
Gleber, S. C., Thieme, W., Chao, W. & Fischer, P. (2009). *J. Microsc.* **235**, 199–208.
Grübel, G., Stephenson, G. B., Gutt, C., Sinn, H. & Tschentscher, T. (2007). *Nucl. Instrum. Methods Phys. Res. B*, **262**, 357–367.
Günther, C. M., Pfau, B., Mitzner, R., Siemer, B., Roling, S., Zacharias, H., Kutz, O., Rudolph, I., Schondelmaier, D., Treusch, R. & Eisebitt, S. (2011). *Nat. Photon.* **5**, 99–102.
Ishikawa, T. *et al.* (2012). *Nat. Photon.* **6**, 540.
Korff Schmising, C. von, Pfau, B., Schneider, M., Günther, C. M., Giovannella, M., Perron, J., Vodungbo, B., Müller, L., Capotondi, F., Pedersoli, E., Mahne, N., Lüning, J. & Eisebitt, S. (2014). *Phys. Rev. Lett.* **112**, 217203.
Lyamayev, V. *et al.* (2013). *J. Phys. B*, **46**, 403–408.

Martin, A. V., D'Alfonso, A. J., Wang, F., Bean, R., Capotondi, F., Kirian, R. A., Pedersoli, E., Raimondi, L., Stellato, F., Yoon, C. H. & Chapman, H. N. (2014). *Nat. Commun.* **5**, 4661.
Masciovecchio, C. *et al.* (2015). *J. Synchrotron Rad.* **22**, 553–564.
Müller, L. *et al.* (2013*a*). *Phys. Rev. Lett.* **110**, 234801.
Müller, L. *et al.* (2013*b*). *Synchrotron Radiat. News*, **26**, 27–32.
Nugent, K. A. (2010). *Adv. Phys.* **59**, 1–99.
Pedersoli, E. *et al.* (2011). *Rev. Sci. Instrum.* **82**, 043711.
Raimondi, L. *et al.* (2013). *Nucl. Instrum. Methods Phys. Res. A*, **710**, 131–138.
Raines, K. S., Salha, S., Sandberg, R. L., Jiang, H., Rodriguez, J. A., Fahimian, B. P., Kapteyn, H. C., Du, J. & Miao, J. (2010). *Nature (London)*, **463**, 214–217.
Riedel, R., Al-Shemmary, A., Gensch, M., Golz, T., Harmand, M., Medvedev, N., Prandolini, M. J., Sokolowski-Tinten, K., Toleikis, S., Wegner, U., Ziaja, B., Stojanovic, N. & Tavella, F. (2013). *Nat. Commun.* **4**, 1731.
Roy, S., Parks, D., Seu, K. A., Su, R., Turner, J. J., Chao, W., Anderson, E. H., Cabrini, S. & Kevan, S. D. (2011). *Nat. Photon.* **5**, 243–245.
Seibert, M. M. *et al.* (2011). *Nature (London)*, **470**, 78–81.
Song, C., Bergstrom, R., Ramunno-Johnson, D., Jiang, H., Paterson, D., de Jonge, M. D., McNulty, I., Lee, J., Wang, K. & Miao, J. (2008). *Phys. Rev. Lett.* **100**, 025504.
Svetina, C., Abrami, A., Cudin, I., Fava, C., Gerusina, S., Gobessi, R., Rumiz, L., Sostero, G., Zangrando, M. & Cocco, D. (2011). *Proc. SPIE*, **8139**, 81390J.
Tripathi, A., Mohanty, J., Dietze, S. H., Shpyrko, O. G., Shipton, E., Fullerton, E. E., Kim, S. S. & McNulty, I. (2011). *Proc. Natl Acad. Sci. USA*, **108**, 13393–13398.
Van der Laan, G. (2013). *J. Phys. Conf. Ser.* **430**, 012127.
Xu, R. *et al.* (2014). *Nat. Commun.* **5**, 4061.
Yoon, C. H., Barthelmess, M., Bean, R. J., Capotondi, F., Kirian, R. A., Kiskinova, M., Pedersoli, E., Raimondi, L., Stellato, F., Wang, F. & Chapman, H. N. (2014). *Opt. Express*, **22**, 8085–8093.
Zangrando, M., Abrami, A., Bacescu, D., Cudin, I., Fava, C., Frassetto, F., Galimberti, A., Godnig, R., Giuressi, D., Poletto, L., Rumiz, L., Sergo, R., Svetina, C. & Cocco, D. (2009). *Rev. Sci. Instrum.* **80**, 113110.